Journal of Energy Storage 119 (2025) 116209

Contents lists available at ScienceDirect

Journal of Energy Storage

journal homepage: www.elsevier.com/locate/est

Research Papers

Optimal sizing and operation of community hybrid energy storage systems☆

Lei Wan [a], Jiajia Yang [b,*], Yu Yang [a], Tao Li [c], Hangyue Liu [d], Fushuan Wen [a]

[a] College of Electrical Engineering, Zhejiang University, Hangzhou 310027, China
[b] College of Science and Engineering, James Cook University, Townsville 4811, Australia
[c] China Energy Economic and Technological Research Institute Co., Ltd., Beijing 102211, China
[d] Sungrow Australia Group Pty. Ltd., Sydney 2060, Australia

ARTICLE INFO

Keywords:
Community energy storage system
Slow-response energy storage device
Fast-response energy storage device
Multi-objective optimization
Community profit
Load fluctuation

ABSTRACT

Configuring a community energy storage system (CESS) helps balance energy supply-demand and increase the self-consumption rate of distributed renewable energy based generation on the user side. However, a CESS primarily relies on battery storage, whose high economic cost makes large-scale development and practical application difficult. Given this background, the optimal sizing and operational strategy for a community hybrid energy storage system (CHESS) is proposed in this paper, which comprises the slow-response energy storage device (SRESD) and the fast-response energy storage device (FRESD). Firstly, considering the community's willingness to deploy storage and the impact of storage on smoothing load fluctuations, a multi-objective optimization model aiming to maximize community profits and minimize load fluctuations is proposed, which is transformed into a single objective optimization by incorporating a penalty factor. Then, the Density-Based Spatial Clustering of Applications with Noise (DBSCAN) algorithm is employed to derive typical community load and electricity price curves which are used to schedule the monthly charge and discharge periods for the SRESD, subsequently developing the optimal sizing and annual 8760-hour operational strategy for a CHESS based on this schedule. On this basis, three storage configurations (CHESS, SRESD, and FRESD) are compared, and it is found by simulation results that the CHESS combines the advantages of both SRESD and FRESD, offering larger arbitrage opportunity with the peak-valley price spread and being more effective in managing load fluctuations. Finally, the impacts of declining battery costs on optimization results are examined and experimental verification based on real data from Australia is carried out, with the feasibility and sustainability of the proposed sizing and operational strategy for a CHESS demonstrated.

Nomenclature

Abbreviations

BESS	Battery energy storage system
CESS	Community energy storage system
CHESS	Community hybrid energy storage system
DBSCAN	Density-Based Spatial Clustering of Applications with Noise
FRESD	Fast-response energy storage device
PTES	Pumped thermal energy storage
PV	Photovoltaics
SRESD	Slow-response energy storage device
WEM	Wholesale electricity market
NSGA-II	Nondominated Sorting Genetic Algorithm II
MOEA/D	Multi-objective Evolutionary Algorithm Based on Decomposition

Parameters

D	Total number of days in a calendar year (365 or 366)
$OF_2^{w/o}$	Sum of the daily standard deviations of net load for the entire year without CHESS deployment
$P_{d,t}^{load}$	Community load at the t-th interval on the d-th day

(continued on next page)

☆ This article is part of a special issue entitled: Hybrid Energy Storage published in Journal of Energy Storage.

* Corresponding author.
E-mail address: jiajia.yang@jcu.edu.au (J. Yang).

https://doi.org/10.1016/j.est.2025.116209
Received 14 December 2024; Received in revised form 14 February 2025; Accepted 11 March 2025
Available online 25 March 2025

(*continued*)

$\overline{P}_d^{w/o}$	Average power within a day without CHESS
r	Discount rate
T	The number of half-hour intervals per day
$\lambda_{d,t}^{WEM}$	WEM price at the t-th time interval on the d-th day
λ_{CRF}^{slow}	Capacity decay factor of SRESD
λ_{CRF}^{fast}	Capacity decay factor of FRESD
γ^{slow}	Planning horizon of SRESD
γ^{fast}	Planning horizon of FRESD
μ^{slow}	Unit capacity investment cost of SRESD
μ^{fast}	Unit capacity investment cost of FRESD
ξ^{slow}	The ratio of the annual O&M cost to the initial investment of SRESD
ξ^{fast}	The ratio of the annual O&M cost to the initial investment of FRESD
η_c	Charging efficiency of SRESD
η_d	Discharging efficiency of SRESD
Δt	Time interval

Variables

β	Penalty factor
$C^{m,w/o}$	Community annual costs without deploying CHESS
$C^{m,w}$	Community annual costs with deploying CHESS
C^{ess}	Annual investment of CHESS
$C^{ess,slow}$	Annual investment of SRESD
$C^{ess,fast}$	Annual investment of FRESD
E^{slow}	Energy capacity of SRESD
E^{fast}	Energy capacity of FRESD
OF_1	Annual revenue with CHESS deployment
OF_2	Sum of the daily standard deviations of net load for the entire year with CHESS deployment
$P^{ess,slow,cap}$	Power capacity of SRESD
$P^{ess,fast,cap}$	Power capacity of FRESD
$\overline{P}_d^{w}$	Average power within a day with CHESS
$P_{d,t}^{ess,slow}$	Charging/discharging power of SRESD at the t-th time interval on the d-th day
$P_{d,t}^{ess,fast}$	Charging/discharging power of FRESD at the t-th time interval on the d-th day
T_n	Charging duration of SRESD
T_m	Discharging duration of SRESD
t_c	Charging start time of SRESD by monthly plan
t_{c+n}	Charging end time of SRESD by monthly plan
t_d	Discharging start time of SRESD by monthly plan
t_{d+m}	Discharging end time of SRESD by monthly plan

1. Introduction

In recent years, rapid advancements in renewable energy generation technologies and significant cost reductions have enabled numerous distributed photovoltaics (PV) to integrate into modern power systems at many user terminals. For instance, Australia added 520 MW of rooftop PV capacity in the first quarter of 2023 [1]. However, the intermittency and variability of power outputs from distributed energy resources (DERs) cause power supply-demand imbalances and pose new challenges to the secure and economic operation of power systems [2]. Therefore, enhancing flexibility of users in providing power regulation is crucial for ensuring secure and reliable power supply as well as promoting the capability of accommodating intermittent renewable energy generation.

In this context, the energy storage as a backup for renewable energy, is expected to play a significant role in modern power systems. However, the high investment costs of energy storage devices, which are one-time expenditures, mean that most storage systems primarily serve for maintaining power system secure operation. Providing storage for individual users yields low returns on investment and results in low utilization rates, leading to significant resource waste [3]. To promote the utilization rate of energy storage devices and the accommodation level of intermittent renewable energy generation, the so-called community energy storage system (CESS) has already undergone pilot studies in countries such as Germany [4] and Australia [5], which can serve large-scale, multi-region user groups, promoting rapid development of commercial storage utilization [6]. Additionally, CESS plays a positive role in providing voltage regulation for distribution networks, enhancing the utilization of DREs [7], and reducing carbon emissions [8]. However, the high costs of current energy storage systems hinder their large-scale and extensive applications [9]. Therefore, optimizing the allocation of energy storage capacity and operational strategy is crucial to ensuring reasonable returns on CESS investments.

Currently, CESSs primarily rely on battery energy storage systems (BESSs), and some research work has been conducted on the optimal sizing of CESSs. The optimization methods for a BESS under different ownership structures based on net present value (NPV) are presented in [8–10]. A capacity optimization framework for a BESS with the objectives of minimizing electricity costs and peak demand is presented in [13], using a price response model. An optimization framework based on machine learning and artificial ecosystem optimization (AEO) algorithms is introduced in [14] to determine the optimal BESS capacity and charge/discharge strategies. An optimization model is presented in [15] that considers both the investment return and operational costs of a BESS, identifying the most cost-effective storage capacity through simulations of various capacity scenarios. A cooperative energy storage business model is developed in [16] based on a sharing mechanism, which determines the optimal energy storage configuration through coalition games.

To account for seasonal fluctuations of wind and solar energy based generation, some studies have considered efficient planning methods over the entire year (8760-h). The optimal sizing problem of PV and BESS in renewable energy communities is investigated in [17], considering the impacts of different battery operation strategies and sizing on the power system. An effective source-grid-storage coordination planning model is introduced in [18], describing hourly operation throughout a year into the multi-time-scale power balance planning of power systems. A design and operational optimization framework for multiple energy systems is presented in [19], including seasonal energy storage. An energy system configuration planning method is proposed in [20] based on time-series coupling. An optimal sizing adjustment method for a CBESS is presented in [21], with the long-term economic performance of community batteries considered.

However, the aforementioned studies have certain limitations. On one hand, the planning process is simplified in [8–14], without considering the full annual operation of storage (8760-h), instead relying on a few representative scenarios for simulations. This approach captures only the characteristics of intermittent renewable energy based generation and load fluctuations under typical conditions, neglecting power variability on longer time scales (weekly, monthly, annually), which may introduce errors compared to planning based on full-year simulations. On the other hand, relying on a limited number of typical scenarios does not accurately reflect the conditions of every natural day throughout the year, particularly for power variations caused by extreme weather events whose fluctuation trends and magnitudes are difficult to capture through typical scenarios. Therefore, methods based on a few typical scenarios for short-term [8–14] or full-year simulations [15–19] are insufficient to ensure an appropriate storage sizing.

Additionally, to further enhance the profitability of a CESS, some studies have explored potential revenue-generating services. An innovative interactive voltage regulation platform for the BESS is presented in [22], which exchanges voltage regulation services with Distribution Network Service Providers (DNSPs). A short-term scheduling method is presented in [23] for the BESS that integrates day-ahead energy and ancillary services markets. Operation strategies for batteries to provide demand response considering community-level disaster recovery are proposed in [24]. Besides, the capability and value of the BESS in providing grid support are analyzed in [25]. Although current commercial models for the CESS are diverse, the profitability remains uncertain and is heavily reliant on subsidies (including government grants and network innovation funding) [26], making it crucial to achieve self-sustaining profitability for large-scale development.

In addition to battery-based storage, some CESSs have also explored other forms of energy storage configurations. a community hybrid energy storage system (CHESS) integrating hydrogen and electricity storage components to enhance the economic and environmental performance of community integrated energy systems is proposed in [27]. A collaborative model for communities, encompassing electricity, heating, cooling, and an emerging hydrogen network equipped with shared hybrid energy storage is developed in [28]. An innovative distributed energy system combining solar energy utilization with hybrid storage technologies is introduced in [29], including thermal and electricity storage. However, the aforementioned studies primarily emphasize the operation of CHESS and their reliance on complex energy forms makes it challenging to achieve economic benefits that are attractive enough for communities to adopt such configurations.

Given the above context, more advanced energy storage technologies/solutions are emerging, and are expected to play a significant role in the CESS, particularly the slow-response energy storage device (SRESD), whose low-cost characteristics can address the limited deployment issues of the CESS [30]. For instance, the pumped thermal energy storage (PTES), which uses excess electricity for heating thermal storage and converts the stored thermal energy into electricity when needed [31], shows potential for small- and medium-scale applications [32]. This paper explores the capacity sizing and operational strategy of a CHESS, including the SRESD represented by PTES and the fast-response energy storage device (FRESD) represented by BESS. The research work in this paper can be summarized as follows:

i. By integrating the SRESD and FRESD, a multi-objective optimization model for a CHESS to maximize community profits and minimize load fluctuations is proposed, thereby enhancing the community's willingness to deploy energy storage.
ii. Utilizing accurate annual 8760-h simulations, the operational strategy for the CHESS is developed, which could effectively enhance community revenue and mitigate the impacts of load fluctuations on the power system.
iii. Based on community net load curves and wholesale electricity market (WEM) price curves, the Density-Based Spatial Clustering of Applications with Noise (DBSCAN) algorithm is employed to derive the typical net load and electricity price curves which are used to schedule the monthly charge and discharge periods for the SRESD.
iv. The proposed method is validated using actual community data from Australia and evaluated against various energy storage solutions, demonstrating the feasibility and sustainability of the proposed sizing and operational strategy for the CHESS.

The structure of this paper is as follows: Section 2 presents the structure and planning framework of a CHESS used in this study. Section 3 examines the impact of the CHESS on community profits and load fluctuations in the distribution network, establishing an 8760-h simulation-based optimization model for the CHESS. Section 4 describes the planning method for the monthly charging and discharging schedule of the SRESD using the DBSCAN algorithm. Section 5 compares various energy storage configurations and investigates the impacts of advancements in battery technology on the CHESS, with analysis and validation provided based on actual community data from Australia. Finally, Section 6 presents conclusions and suggests future research in this field.

2. Problem description

2.1. Structure of the community microgrid

This paper focuses on a CHESS that integrates both SRESD (such as PTES) and FRESD (such as BESS), as depicted in Fig. 1. On the supply side, the system includes rooftop PV arrays within the community and the local grid. The distributed PV generation system and the local grid are connected to the AC bus via inverters and transformers, respectively, allowing for the surplus PV energy to be fed back into the grid. On the load side, the system includes both fixed loads and flexible loads such as electric vehicles (EVs). Additionally, both SRESD and FRESD are connected to the bus via inverters, enabling the community to perform peak shaving and load balancing.

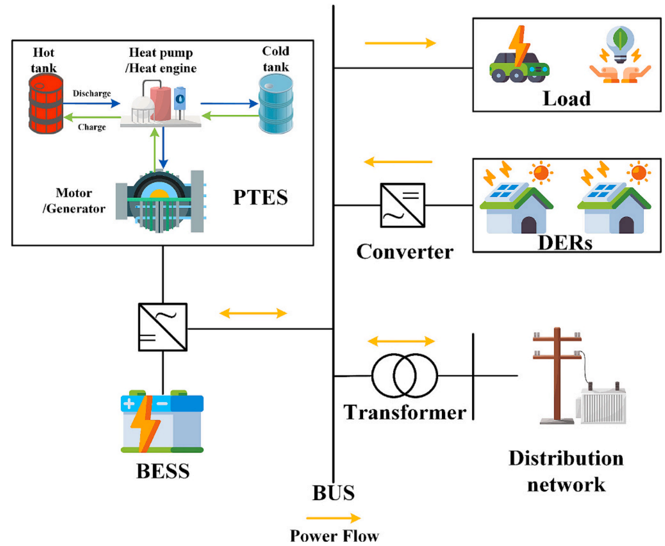

Fig. 1. Community microgrid structure.

2.2. Sizing and operation framework of the CHESS

As illustrated in Fig. 2, the proposed CHESS sizing and operation framework includes four components: the planning of the SRESD operating schedules, the CHESS economic planning model, the load fluctuation optimization model, and the optimization model solution. The framework utilizes the DBSCAN algorithm to extract typical community daily net load curves for every month and determines the monthly operating schedules for the SRESD in conjunction with WEM prices. To ensure the community profitability while addressing the requirements of the distribution network, a multi-objective optimization model for a CHESS with the annual 8760-h simulation and load fluctuation evaluation is developed. By introducing penalty factors, the multi-objective model is converted into a single-objective model for solution, leading to the determination of the optimal CHESS sizing and operational strategy.

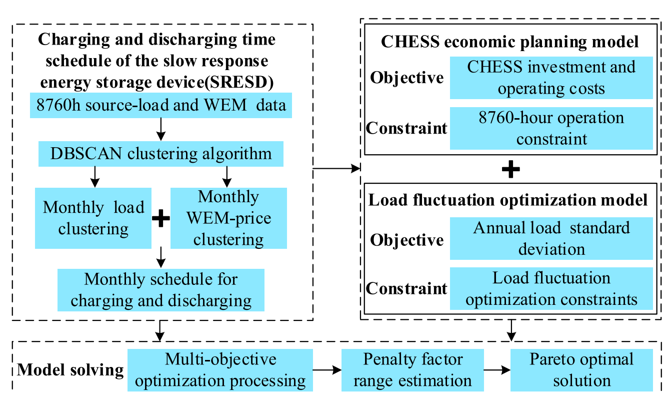

Fig. 2. Sizing and operation framework of CHESS.

3. Mathematical formulation

A mathematical model for the sizing and operational strategy of the CHESS is developed in this section, based on accurate annual 8760-h simulations, with both the investment and operational costs of storage systems considered and the need for load fluctuation smoothing addressed.

3.1. Objective functions

Economic feasibility remains a crucial factor for the community when selecting energy storage systems. It is necessary to compare the community costs before and after the implementation of the CHESS, with the difference representing the realized profits from the CHESS deployment. Therefore, the objective function for community profits is defined as:

$$max\ \ OF_1 = C^{m,w/o} - C^{m,w} \tag{1}$$

$$C^{m,w/o} = \sum_{d=1}^{D}\sum_{t=1}^{T} P_{d,t}^{load}\lambda_{d,t}^{WEM}\Delta t \tag{2}$$

$$C^{m,w} = \sum_{d=1}^{D}\sum_{t=1}^{T}\left(P_{d,t}^{load} + P_{d,t}^{ess,slow} + P_{d,t}^{ess,fast}\right)\lambda_{d,t}^{WEM}\Delta t + C^{ess} \tag{3}$$

$$C^{ess} = C^{ess,slow} + C^{ess,fast} \tag{4}$$

$$C^{ess,slow} = \lambda_{CRF}^{slow}\mu^{slow}E^{slow} + \xi^{slow}\mu^{slow}E^{slow} \tag{5}$$

$$C^{ess,fast} = \lambda_{CRF}^{fast}\mu^{fast}E^{fast} + \xi^{fast}\mu^{fast}E^{fast} \tag{6}$$

$$\lambda_{CRF}^{slow} = \frac{r(1+r)^{\gamma_{slow}}}{(1+r)^{\gamma_{slow}} - 1} \tag{7}$$

$$\lambda_{CRF}^{fast} = \frac{r(1+r)^{\gamma_{fast}}}{(1+r)^{\gamma_{fast}} - 1} \tag{8}$$

The objective function Eq. (1) represents the annual profits from deploying energy storage within the community, calculated as the difference in community costs before and after implementing the CHESS. This difference is equivalent to the arbitrage revenue derived from peak-valley electricity prices. A community equipped with the CHESS functions as both a producer and consumer of electricity, thereby actively participating in the WEM. Therefore, Eq. (2) denotes the community cost of participating in the WEM without the CHESS. The community cost with CHESS is divided into two components: the cost of participating in the WEM and the annual costs of storage deployment, as shown in Eq. (3). The annual cost of the CHESS deployment, including both investment and operational costs, is detailed in Eqs. (4)–(6) [33]. Besides, Eqs. (7) and (8) represent the capacity degradation factor, which allocates the total investment across each year.

In addition to considering the community profits from deploying the CHESS, it is crucial to also account for the technical benefits it brings [34]. The storage configuration should not exacerbate fluctuations in net load, which is the most immediate impact of an energy storage on the distribution system. Moreover, accounting for that standard deviation is a well-regarded measure for assessing data volatility in power systems [35], the standard deviation of net load is used as an indicator of load fluctuation as shown in Eq. (9). A smaller standard deviation implies smoother load fluctuations and a stronger capability for the community to self-consume renewable energy. The average daily load after deploying the CHESS is represented in (10). Given that Eq. (9) is a nonlinear objective function, it can be converted into a norm form for the solver computation. Thus, the objective of minimizing load fluctuations can be expressed as Eq. (11).

$$min\ \ OF_2 = \sum_{d=1}^{D}\sqrt{\sum_{t=1}^{T}\left(P_{d,t}^{load} + P_{d,t}^{ess,slow} + P_{d,t}^{ess,fast} - \overline{P}_d^{w}\right)^2 \Big/ T} \tag{9}$$

$$\overline{P}_d^{w} = \frac{\sum_{t=1}^{T} P_{d,t}^{load} + P_{d,t}^{ess,slow} + P_{d,t}^{ess,fast}}{T} \tag{10}$$

$$min\ \ OF_2 = \frac{\sum_{d=1}^{D}\left\|\sum_{t=1}^{T}\left(P_{d,t}^{load} + P_{d,t}^{ess,slow} + P_{d,t}^{ess,fast} - \overline{P}_d^{w}\right)\right\|_2^2}{\sqrt{T}} \tag{11}$$

3.2. Technical limitation and operating constraints

Due to its inherent characteristics, the SRESD cannot adjust charging and discharging power in real-time, with its response time typically being on the minute scale or longer [9], necessitating the pre-planning of its operational schedule. For ease of regulation, this paper employs the SRESD to perform charging and discharging at a constant power during fixed time periods each month, with a daily cycle occurring once per day [36]. The approach is specifically detailed as follows:

$$P_{d,t_c}^{ess,slow} = P_{d,t_{c+1}}^{ess,slow} = \cdots = P_{d,t_{c+n}}^{ess,slow} \tag{12}$$

$$P_{d,t_d}^{ess,slow} = P_{d,t_{d+1}}^{ess,slow} = \cdots = P_{d,t_{d+m}}^{ess,slow} \tag{13}$$

Eqs. (12) and (13) respectively represent the constant charging and discharging power of the SRESD during fixed time periods. The monthly operation scheduling plan is detailed in Section 4.

To ensure the safe and stable operation of the system, it is necessary that both SRESD and FRESD return to their initial daily states after each cycle. Therefore, the total daily charging and discharging power is set to zero, as shown in Eqs. (14) and (15), which are written independently for each d-th design day, decoupling each day from both the previous and the next [19]. When considering the charging and discharging efficiency of the FRESD, binary integer variables would inevitably need to be introduced to distinguish between charging and discharging power while ensuring that both processes do not occur simultaneously. Besides, since this study involves 8760-h simulations, incorporating efficiency would transform the problem into an extremely large-scale mixed-integer problem, which is challenging for solvers to address directly. To avoid the computational complexity with considering that the efficiency of the FRESD approaches 100 % [37] and its energy capacity is designed with sufficient margin, the charging and discharging efficiency of FRESD is ignored for simplification.

$$\int_{t_c}^{t_{c+n}} P_{d,t}^{ess,slow}\eta_c dt + \int_{t_d}^{t_{d+m}} P_{d,t}^{ess,slow}\Big/\eta_d dt = 0 \tag{14}$$

$$\int_T P_{d,t}^{ess,fast} dt = 0 \tag{15}$$

The charging and discharging power of the SRESD and the FRESD are constrained by maximum power limits, as indicated in Eqs. (16) and (17).

$$-P^{ess,slow,cap} \le P_{d,t}^{ess,slow} \le P^{ess,slow,cap} \tag{16}$$

$$-P^{ess,fast,cap} \le P_{d,t}^{ess,fast} \le P^{ess,fast,cap} \tag{17}$$

Based on the security margin for energy storage capacity (0.1 SOC to 0.9 SOC) [38], the capacity sizing constraints that ensures the SRESD and the FRESD operate effectively under extreme conditions are developed. For the SRESD, the extreme condition is defined as operating at maximum power during specified charging or discharging periods, with its capacity traversing the entire security margin, as shown in Eq. (18). However, for the FRESD, the extreme operation condition involves running at maximum charging power for half a day and at maximum discharging power for the other half, which is modeled by Eq. (19).

$$0.8E^{slow} = max\left\{ \int_{t_c}^{t_{c+n}} P^{ess,slow,cap}\eta_c dt, \int_{t_d}^{t_{d+m}} P^{ess,slow,cap} \Big/ \eta_d dt \right\} \tag{18}$$

$$0.8E^{fast} = \int_{T/2} P^{ess,fast,cap} dt \tag{19}$$

Both SRESD and FRESD have capacity state constraints, as outlined in Eqs. (20) and (21). Besides, the capacity states of the SRESD and the FRESD during the optimization period are modeled by Eqs. (22) and (23).

$$0.1E^{slow} \leq E_{d,t}^{slow} \leq 0.9E^{slow} \tag{20}$$

$$0.1E^{fast} \leq E_{d,t}^{fast} \leq 0.9E^{fast} \tag{21}$$

$$E_{d,t}^{fast} = E_{d,t-1}^{fast} + P_{d,t}^{ess,fast}\Delta t \tag{22}$$

$$E_{d,t}^{slow} = \begin{cases} E_{d,t-1}^{slow} + P_{d,t}^{ess,slow}\eta_c\Delta t, & \text{if } t \in (t_c \sim t_{c+n}) \\ E_{d,t-1}^{slow} + P_{d,t}^{ess,slow} \Big/ \eta_d\Delta t, & \text{if } t \in (t_d \sim t_{d+m}) \\ E_{d,t-1}^{slow}, & \text{else} \end{cases} \tag{23}$$

3.3. Problem solving

Common algorithms such as Nondominated Sorting Genetic Algorithm II (NSGA-II) and Multi-objective Evolutionary Algorithm Based on Decomposition (MOEA/D) are widely used for finding Pareto solutions in bi-objective optimization problems. However, the current study involves a high-dimensional multi-objective optimization model for CHESS configuration over 8760 h with applying NSGA-II or MOEA/D in this context would lead to dimensionality issues [39]. Therefore, to balance the profits of CHESS configurations with the impact of load fluctuations on the system, the penalty factor β is introduced to reformulate the multi-objective optimization of Eqs. (1) and (11) with constraints into a single objective optimization problem [40], as given by Eq. (24). After this transformation, the optimization solver can be used to obtain the Pareto solutions, each of which is mathematically optimal.

$$\begin{cases} min & -OF_1 + \beta^* OF_2 \\ \text{s.t.} & (12)-(23) \end{cases} \tag{24}$$

To encourage the adoption of the CHESS in communities, Eq. (25) is employed to ensure positive profits from storage deployment. Additionally, the load fluctuations after implementing the CHESS should not be more severe than those experienced without the CHESS, as represented by Eq. (26), with Eq. (27) showing the daily average load without the CHESS.

$$OF_1 \geq 0 \tag{25}$$

$$OF_2 \leq OF_2^{w/o} = \sum_{d=1}^{D} \sqrt{\sum_{t=1}^{T} \left(P_{d,t}^{load} - \overline{P}_d^{w/o}\right)^2 \Big/ T} \tag{26}$$

$$\overline{P}_d^{w/o} = \frac{\sum_{t=1}^{T} P_{d,t}^{load}}{T} \tag{27}$$

Initially, the penalty factor β is set to zero and incremented in large-step size for testing. The upper limit of the penalty factor can be determined from Eq. (25), while the lower limit is determined from Eq. (26). Once the range for β is identified, the step size is reduced to refine the search and obtain a denser set of Pareto-optimal solutions, and the smaller the step size, the denser the obtained Pareto optimal solutions. In summary, the model leverages penalty factors to transform the multi-objective optimization problem into a single-objective formulation, achieving precise Pareto-optimal solutions.

4. Scheduling of the SRESD operations

Due to lower investment costs, the SRESD primarily serve the purposes of integrating renewable energy and arbitraging peak-valley price spreads. To determine its operational scheduling, it is essential to consider variations in community load and energy prices. This section introduces the operational scheduling process for the SRESD based on community load data [41] and WEM data [42] from Australia, as illustrated in Fig. 3.

To mitigate noise interference and improve the identification of diverse curve patterns, daily load curves from the entire year are treated as individual data points and clustered using the DBSCAN algorithm [43,44] based on their Euclidean distances. Then, the cluster with the most samples is selected, excluding noise points, and its average load curve represents a typical daily load curve. The charging duration T_n for the SRESD is determined using the negative periods of this typical daily load curve, during which the renewable energy generation exceeds community electricity demand. For instance, as shown in Fig. 4-a, the charging duration is 6.5 h in this paper.

Based on Eq. (18), to maximize the utilization of the SRESD and prevent loss of arbitrage opportunities, it is essential to ensure that the sizing in both extreme scenarios are as similar as possible, as indicated in Eq. (28). Consequently, Eq. (29) can be derived to determine the discharging duration T_m based on the established charging duration T_n. In this paper, with a charge-discharge efficiency of 79 % [31], the discharging duration is set to 4 h.

$$\int_{t_c}^{t_{c+n}} P^{ess,slow,cap}\eta_c dt \approx \int_{t_d}^{t_{d+m}} P^{ess,slow,cap} \Big/ \eta_d dt \tag{28}$$

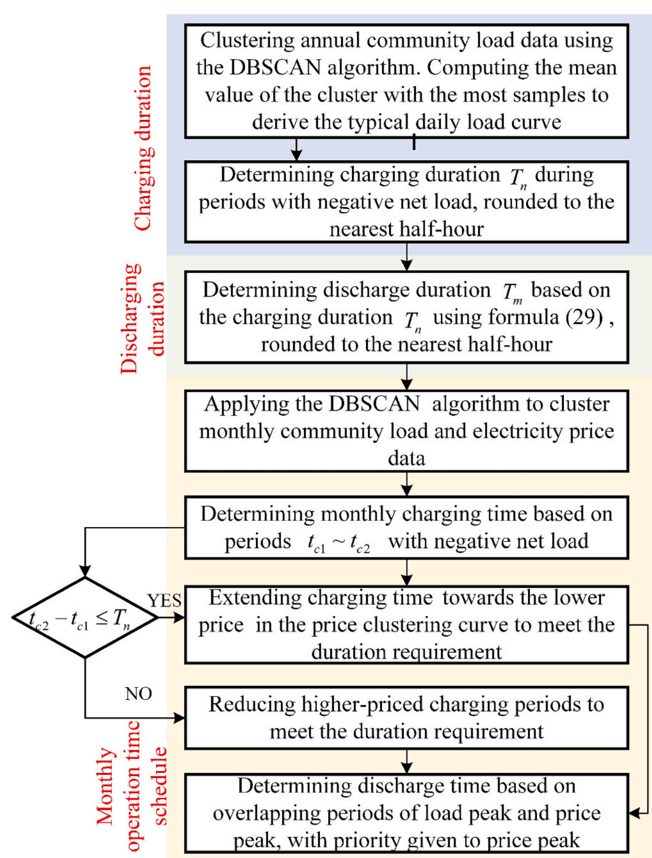

Fig. 3. Scheduling method for the SRESD operation time.

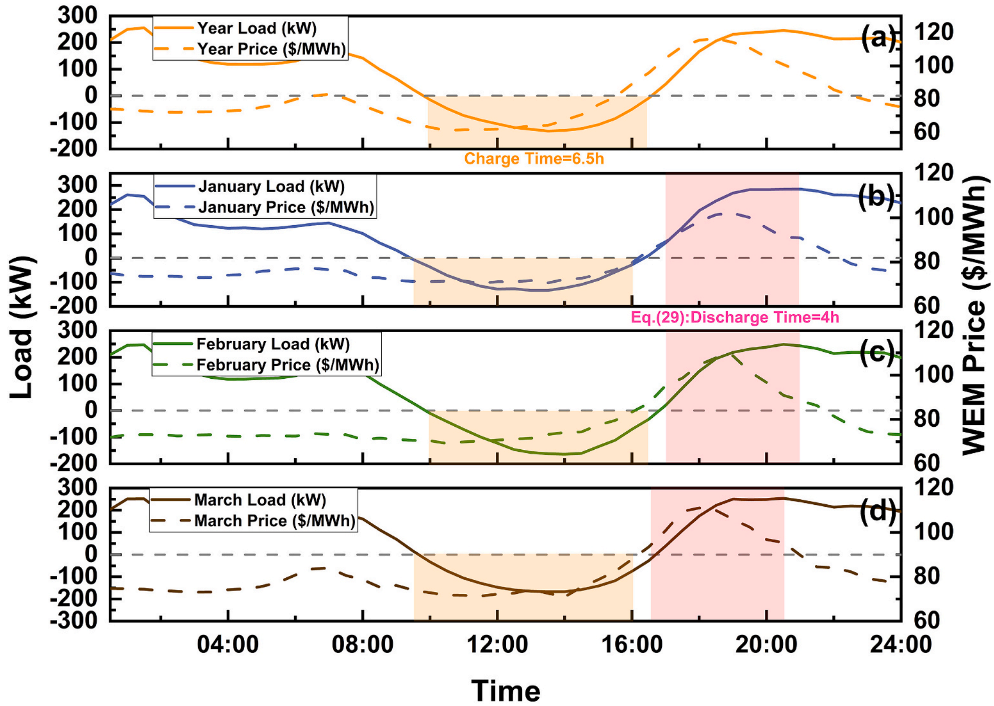

Fig. 4. Load and WEM price clustering curves based on annual and monthly data. (a) Year; (b) January; (c) February; (d) March.

$$T_n\eta_c = (t_{c+n} - t_c)\eta_c \approx (t_{d+m} - t_d)/\eta_d = T_m/\eta_d \quad (29)$$

Finally, based on monthly load and price data clustering, the charging and discharging time for each month is determined. The charging time is prioritized during periods with negative net loads, and if these periods are shorter than the required charging duration T_n, extending charging time towards the lower price in the price clustering curve to meet the duration requirement. Conversely, high-priced charging periods are reduced to meet the duration requirement. Moreover, the discharge time is selected based on the overlap of peak load and peak price periods, with priority given to price peak. Fig. 4-b\c\d illustrates the load and price clustering curves and their corresponding charging and discharging time for January to March, and the annual schedule for the SRESD charging and discharging time is shown in Table 1.

5. Results analysis and discussions

Community load data from 300 users alongside WEM price data from Australia [41,42] are employed in this paper, and the load data encompasses net load information from distributed PV generation, fixed loads, and flexible loads. The primary parameters are detailed in Table 2, where the penalty factor β is determined by constraints Eqs. (25) and (26), which is appropriately extended with increments of 0.005. Computational simulations are performed using MATLAB with the Gurobi solver, on an Intel(R) Core(TM) i9-12900K processor operating at 2.50 GHz, equipped with 16 cores, 128.0 GB RAM, and a 64-bit version of Windows 10.

Table 1
The charging and discharging time schedule for the SRESD.

Month	Charging time	Discharging time
1	9:30–16:00	17:00–21:00
2	10:00–16:30	17:00–21:00
3	9:30–16:00	16:30–20:30
4	9:00–15:30	17:00–21:00
5	9:00–15:30	16:00–20:00
6	9:00–15:30	16:30–20:30
7	9:00–15:30	16:30–20:30
8	9:00–15:30	17:00–21:00
9	9:00–15:30	17:00–21:00
10	9:30–16:00	17:00–21:00
11	9:30–16:00	17:30–21:30
12	9:00–15:30	17:00–21:00

Table 2
The characteristic parameters for the SRESD and the FRESD.

Parameters	Unit	Value
Discount rate (r) [37]	%	3
Calendric life of SRESD (γ^{slow}) [45]	year	30
Calendric life of FRESD (γ^{fast}) [37]	year	15
Capital cost of SRESD (μ^{slow}) [46]	$/kWh	70
Capital cost of FRESD (μ^{fast}) [37]	$/kWh	200
O&M coefficient of SRESD (ξ^{slow}) [47]	%	1.5
O&M coefficient of FRESD (ξ^{fast}) [48]	%	1
Charge efficiency of SRESD (η_c) [31]	%	79
Discharge efficiency of SRESD (η_d) [31]	%	79
Penalty factor (β)	–	0.2–0.9 (S:0.005)
Days of one year (D)	day	365
Optimization period of one day (T)	0.5 h	48

To validate the CHESS sizing and operation strategy model developed in Section 3, the simulation scenarios focus on maximizing the profits of the CHESS deployment and minimizing community load fluctuations. These two objectives are inherently conflicting, as maximizing community profits through peak-valley price arbitrage increases load fluctuations, while minimizing load fluctuations reduces community profits.

5.1. Solution results

5.1.1. Pareto front

The optimal Pareto front for the test scenario is presented in Fig. 5. Utilizing the Gurobi solver ensures that each point on the Pareto front represents an exact optimal solution, strictly adhering to the constraints of the mathematical model presented in Section 3. When configuring

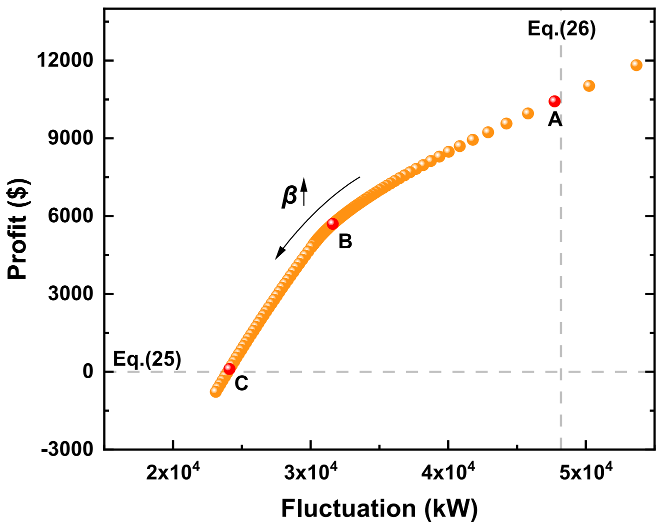

Fig. 5. Pareto front produced by the proposed approaches.

CHESS, there is a trade-off between mitigating load fluctuations and maximizing community revenue, as they are inversely related. Higher economic profits tend to exacerbate load fluctuations, while reducing load fluctuations often comes at lower profits. Moreover, given constraints Eqs. (25) and (26), every solution within the feasible region defined by these constraints represents a viable option for enhancing both the economic and technical benefits of the CHESS.

Table 3 provides the numerical results for points A, B, and C, as illustrated in Fig. 5. The maximum community profit is $10,425.67 at point A, whereas the minimum community load fluctuation is 24,103.65 kW at point C. The selected balance point (point B) yields a profit of $5701.52 and a load fluctuation of 31,611.04 kW. Compared to point A, the community profit at point B decreases by 45.31 %, while the load fluctuation decreases by 33.78 %. In comparison to point B, point C shows a 98.13 % reduction in community profit and a 23.75 % reduction in load fluctuation. The result indicates that, in the context of the CHESS sizing and operational strategy, community profit is more sensitive to changes than load fluctuation, and this sensitivity becomes more pronounced as the penalty factor increases.

5.1.2. The CHESS sizing and cost analysis

Fig. 6-a illustrates the capacity, as well as the maximum charge and discharge power sizing for the SRESD and the FRESD. As the penalty factor increases, the capacity and power sizing of the SRESD gradually decreases. However, the sizing of the FRESD exhibits two distinct trends: initially, both capacity and power sizing are zero, but they increase in the latter half once the penalty factor reaches around 0.71. This behavior is attributed to the higher cost of the FRESD, which is primarily used for regulating load fluctuations. Therefore, when the penalty factor is low (emphasizing community profit), the inclination to configure the FRESD is minimal. However, as the penalty factor increases (emphasizing load fluctuation suppression), the configuration of the FRESD begins.

This is further evidenced by Fig. 6-b, which shows a distinct inflection point in the load fluctuation curve when the penalty factor reaches 0.71. This inflection point signifies the minimum load fluctuation regulation achievable with the SRESD configuration, thus requiring an

Table 3
Comparison of outcomes at different points on the Pareto front.

Solution	Profits ($)	Fluctuations (kW)
A	10,425.6664	47,734.9585
B	5701.5172	31,611.0366
C	106.4479	24,103.6469

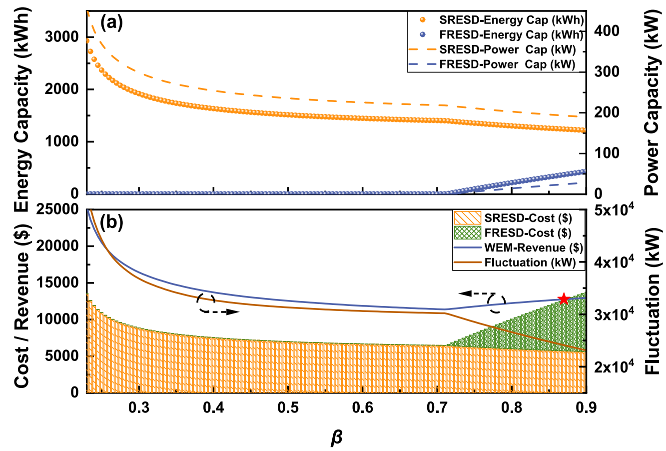

Fig. 6. The CHESS sizing and cost analysis under different penalty factors. (a) Capacity sizing; (b) cost and fluctuation

increase in the FRESD capacity to more effectively suppress load fluctuations. Moreover, the revenue curve from the WEM demonstrates that, as the penalty factor increases, the cost of the SRESD gradually decreases. However, due to the high cost of the FRESD, peak-valley arbitrage does not generate profit, resulting in no inclination to deploy the FRESD at the initial stage, thus the cost remains zero. When the penalty factor increases to 0.71, the load fluctuations begin to decrease significantly, while the community's profits also declines rapidly. Notably, the intersection (point star) of the revenue curve and the CHESS configuration cost represents the optimal point for regulating load fluctuations with only $106.4479. profits, corresponding to point C in Fig. 5.

5.1.3. 8760-hour operation strategy for the CHESS

The operating strategy for the CHESS with maximum profit (point A in Fig. 5) is illustrated in Fig. 7. At this point, the SRESD has an energy capacity of 2577 kWh and a power capacity of 401 kW, while the FRESD has no capacity configured. Fig. 7-a depicts the community load after configuring the CHESS, while Fig. 7-b illustrates the original load without the CHESS, revealing no improvement in load fluctuation. The annual operation strategy for the SRESD is presented in Fig. 7-c, with significant charge-discharge power variations, aiming to maximize peak-valley price spread arbitrage in the WEM. Fig. 7-d displays the annual operation strategy for the FRESD, where the power remains at

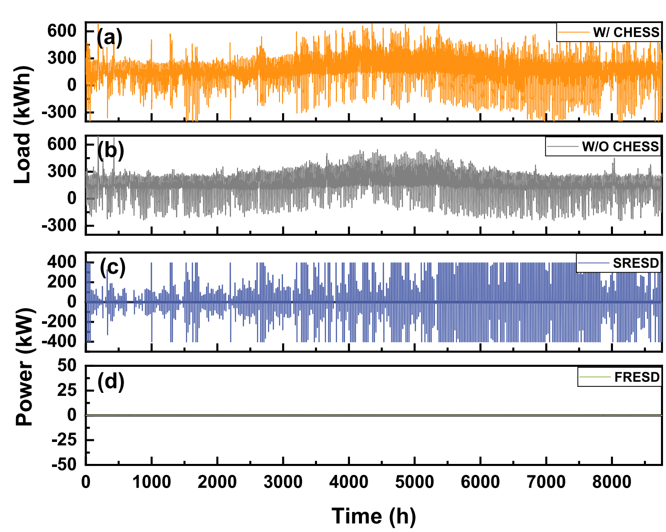

Fig. 7. The CHESS operation strategy with maximum profit (point A in Fig. 5). (a) Load with the CHESS; (b) load without the CHESS; (c) charge/discharge power of the SRESD; (d) charge/discharge power of the FRESD.

zero due to lack of configuration under high-profit expectations.

The operating strategy for the CHESS with minimum load fluctuation (point C in Fig. 5) is presented in Fig. 8. At this point, the SRESD has an energy capacity of 1240 kWh and a power capacity of 193 kW, while the FRESD has an energy capacity of 369 kWh and a power capacity of 25 kW. Fig. 8-a illustrates the community load after implementing the CHESS, compared to the original load without the CHESS in Fig. 8-b, demonstrating a significant reduction in load fluctuations, approximately by 49.98 %. The 8760-h charge and discharge strategies for the SRESD and the FRESD are illustrated in Fig. 8-c and -d, respectively.

Additionally, as shown in Fig. 9, further observations are made on May 31 and June 1 under conditions of minimum load fluctuation (point C in Fig. 5). Fig. 9-a illustrates the impact of the CHESS on load during these two days, showing a significant reduction in load fluctuation. Fig. 9-b shows that on May 31, from 09:00 to 15:30, the SRESD charges at a constant power during the original load's valley period, and discharges at a constant power from 16:00 to 20:00 during the original load's peak period, effectively flattening the load peaks and valleys. The operation of the SRESD also aligns with the peaks and valleys of the WEM price curve, indicating potential for arbitrage opportunities. Besides, supplementary configuration of the FRESD further improves load fluctuation. On June 1, although peak-valley arbitrage shifts the load peak and valley periods, the overall load fluctuation is still reduced. Besides, this is the opposite of the typical peak and valley periods in a traditional distribution network, which helps stabilize the overall load fluctuations of the system, demonstrating the effectiveness of this method.

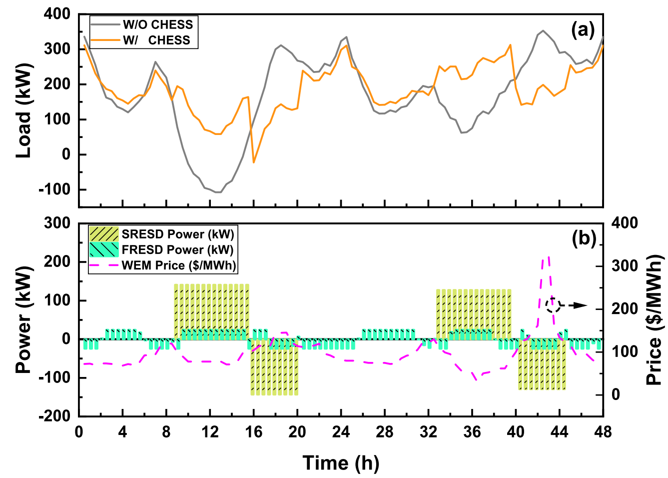

Fig. 9. Operating conditions from May 31 to June 1 in 2013 under minimum load fluctuation (point C in Fig. 5). (a) Load; (b) CHESS

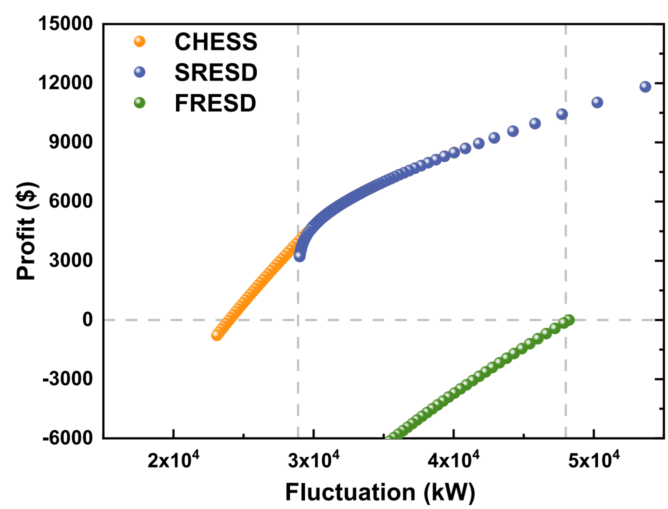

Fig. 10. Pareto fronts under different configuration schemes.

5.2. Comparison and analysis

5.2.1. Comparison of different configuration schemes

Three different energy storage configuration schemes are compared and analyzed in this paper:

- Configuring the SRESD and the FRESD (CHESS);
- Configuring the SRESD;
- Configuring the FRESD.

Fig. 10 shows that configuring the SRESD can yield some community profits and regulate load fluctuations. However, its adjustment capability is limited, with a minimum optimization of load fluctuations up to 28,900 kW. In contrast, configuring the FRESD is highly effective at regulating load fluctuations, but its high cost prevents it from benefiting from peak-valley price spread arbitrage, resulting in negative profits. Nevertheless, the CHESS combines the advantages of both SRESD and FRESD, offering a greater range for regulating load fluctuations compared to the SRESD, and achieving positive profits in contrast to the FRESD. Therefore, configuring the CHESS is the superior choice for community energy storage. Notably, The initial part of the CHESS Pareto fronts curve overlaps with the SRESD curve because the FRESD within the CHESS has no configuration intention under high profit expectations.

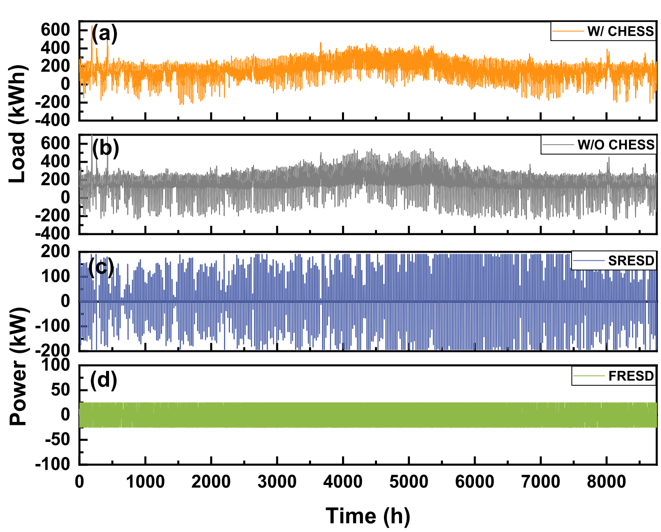

Fig. 8. The CHESS operation strategy with minimum load fluctuation (point C in Fig. 5). (a) Load with the CHESS; (b) load without the CHESS; (c) charge/discharge power of the SRESD; (d) charge/discharge power of the FRESD.

5.2.2. Impact of battery cost development on the CHESS configuration

According to the findings presented in [49], the cost of battery is expected to decrease due to advancements of battery raw materials mining and manufacturing technologies, reaching an estimated 100 $/kWh by 2025. To account for this trend, three cases are analyzed in this paper:

- Case 1: with the FRESD capital price of 200 $/kWh;
- Case 2: with the FRESD capital price of 150 $/kWh;
- Case 3: with the FRESD capital price of 100 $/kWh.

The Pareto curves for the three cases are illustrated in Fig. 11. It is evident that Case 3 achieves the optimal balance between maximizing

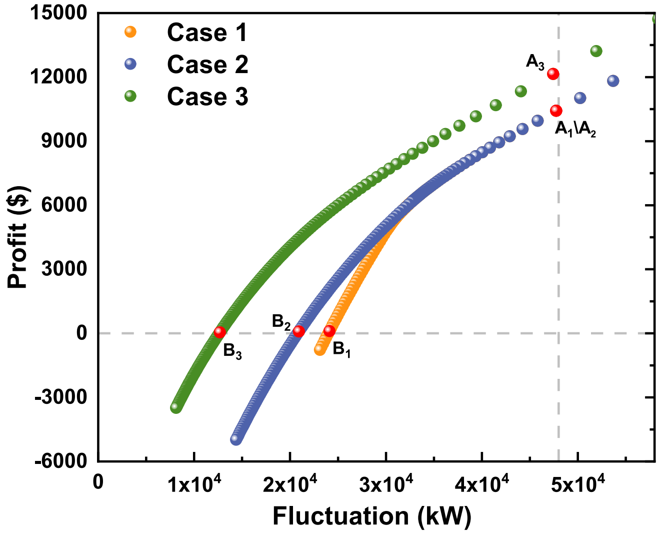

Fig. 11. Pareto fronts under the different FRESD cost.

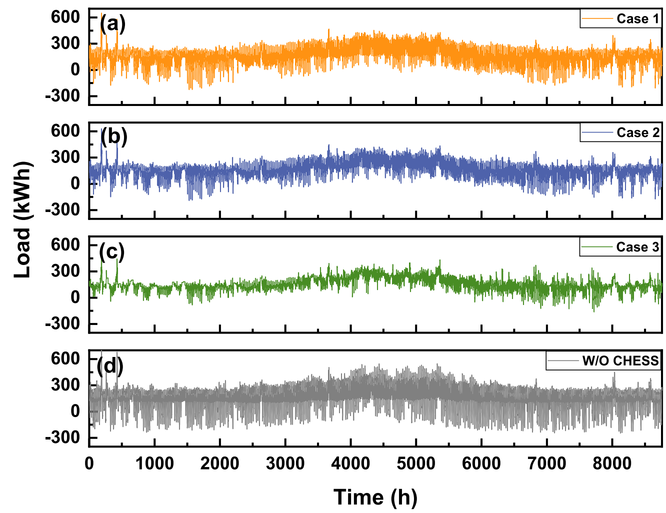

Fig. 12. Community load fluctuations with minimum load fluctuation under different cases (point B_1, B_2, B_3 in Fig. 11). (a) Case1; (b) Case2; (c) Case3; (d) without the CHESS.

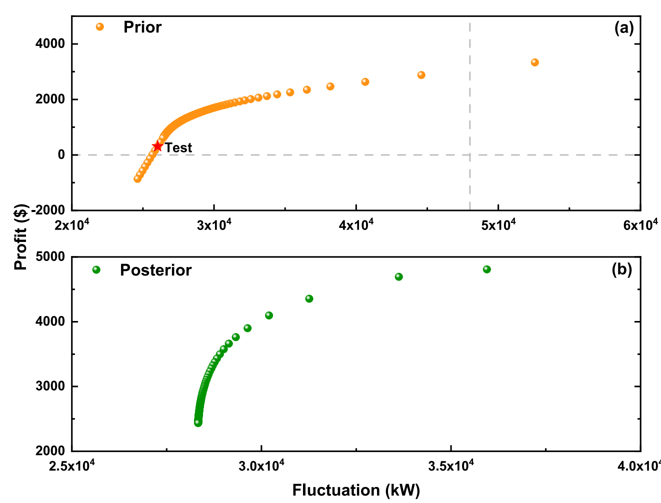

Fig. 13. Pareto fronts based on prior and posterior data. (a) Prior; (b) posterior.

community profit and minimizing load fluctuation, owing to the lowest FRESD cost, which facilitates effective peak-valley price spread arbitrage. Moreover, further analysis reveals based on Eqs. (1)–(3) that the price at which peak-valley price spread arbitrage balances with the FRESD costs is approximately 129$/kWh.

When comparing Case 1 and Case 2 under high profit expectations, the FRESD costs remain prohibitively high, resulting in zero willingness to configure the FRESD, which caused the Pareto curves for both cases overlap. Conversely, under expectations of lower load fluctuations, Case 2 performs better because its lower cost facilitates a more favorable trade-off between reducing load fluctuations and sacrificing profit margins.

Specifically, Table 4 presents the configuration schemes for the special points illustrated in Fig. 11. It is evident that Case 3 achieves a maximum benefit that is 16.54 % higher than that of the other two cases when comparing A_1, A_2, and A_3. Besides, in the context of minimizing load fluctuations, the ratios of energy capacity between SRESD and FRESD under B_1, B_2, and B_3 are 3.36, 1.67, and 0.47, respectively. The increasing proportion of energy capacity allocated to the FRESD indicates that the FRESD is more effective at managing load fluctuations compared to the SRESD, although cost constraints limit its configuration. Furthermore, Fig. 12 demonstrates the community load under B_1, B_2, and B_3, demonstrating that Case 3 has a superior capability for controlling load fluctuations while maintaining similar profits.

5.2.3. Sustainability verification

To validate the enduring value of this method, two consecutive years of load data from 300 users, along with WEM price data are utilized in this paper. The data from the first year is used as prior information to determine the CHESS energy capacity sizing. Then, based on this determined capacity sizing, the second year's data is used as posterior information to develop the 8760-h operational strategy using the proposed model, evaluating the economic and social benefits of the CHESS.

Fig. 13-a shows the Pareto front generated using the prior data. As PV capacity increases and system fluctuations become more pronounced, a randomly selected test point from Fig. 13-a, which demonstrates better load fluctuation adjustment ability, has the configuration of the SRESD with 1109 kWh and FRESD with 47 kWh.

As shown in Fig. 13-b, simulating the configuration of the test points with the posterior data demonstrates that even with the maximum benefit (approximately 4808$), the method effectively mitigates load fluctuations. Moreover, with the minimum load fluctuation (approximately 28,322 kW), the method also yields significant economic benefits. Thus, the sizing and operational strategy developed by this paper

Table 4
Comparison of special configuration schemes under different cases.

Solution	Profit ($)	Fluctuation (kW)	SRESD power capacity (kW)	SRESD energy capacity (kWh)	FRESD power capacity (kW)	FRESD energy capacity (kWh)
A_1	10,425.6664	47,734.9585	401	2577	0	0
A_2	10,425.6664	47,734.9585	401	2577	0	0
A_3	12,149.6005	47,420.6270	349	2239	100	1506
B_1	106.44786	24,103.6469	193	1240	25	369
B_2	91.9034	20,914.0063	181	1161	46	696
B_3	46.7971	12,680.0066	123	790	112	1679

exhibit sustainable effectiveness.

6. Conclusions

The sizing and operational strategy for the CHESS, composed of the SRESD and the FRESD, was proposed to address the challenge of high costs that hinder large-scale development and application. Initially, a multi-objective model was developed to maximize community profits and minimize load fluctuations, based on a community microgrid framework. Then, the DBSCAN algorithm was employed to derive the typical community load and electricity price curves which were used to schedule the monthly charge and discharge periods for the SRESD, subsequently developing the optimal sizing and 8760-h operational. Finally, an experimental analysis based on actual community load and electricity price data from Australia led to the following conclusions:

(1) The CHESS offers a significant cost advantage over the FRESD, providing greater arbitrage opportunities from peak-valley price spreads and thereby can help promote the large-scale development of community energy storage.
(2) The primary advantage of the SRESD lies in arbitrage of peak-valley electricity prices, while it can also somewhat reduce community load fluctuations through optimized operational strategies. In contrast, the FRESD is more effective in regulating load fluctuations.
(3) As the cost of battery storage systems decreases, the FRESD may directly balance its cost through arbitrage in peak-valley price spread. This paper finds that the battery price at which arbitrage balances with the FRESD costs is approximately 129$/kWh.
(4) The configuration scheme derived from prior data continues to yield high profits and effective load fluctuation control when tested with posterior data, verifying the sustainability of the sizing and operational strategy developed by this paper.

This paper demonstrates the theoretically promising value of the CHESS. Future research should explore its application in various electricity markets and further investigate configuration methods for the CHESS in higher voltage level distribution networks.

CRediT authorship contribution statement

Lei Wan: Writing – original draft, Software, Methodology, Conceptualization. **Jiajia Yang:** Resources, Methodology. **Yu Yang:** Writing – review & editing, Methodology. **Tao Li:** Resources. **Hangyue Liu:** Writing – review & editing. **Fushuan Wen:** Writing – review & editing.

Declaration of competing interest

The authors declare that they have no known competing financial interests or personal relationships that could have appeared to influence the work reported in this paper.

Acknowledgements

This work is supported by National Key Research and Development Program of China (2022YFB2403100) and China Energy Investment Corporation Science and Technology Project (Grant No. GJPT-23-21).

Data availability

No data was used for the research described in the article.

References

[1] Australian Energy Council, Solar report. https://www.energycouncil.com.au/media/buqozv3k/australian-energy-council-solar-report-q1-2023.pdf, 2023. (Accessed 30 July 2024).
[2] N.A. Ibrahim, S.R. Wan Alwi, Z.A. Manan, A.A. Mustaffa, K. Kidam, Risk matrix approach of extreme temperature and precipitation for renewable energy systems in Malaysia, Energy 254 (2022) 124471, https://doi.org/10.1016/j.energy.2022.124471.
[3] D. Zhao, H. Wang, J. Huang, X. Lin, Virtual energy storage sharing and capacity allocation, IEEE Trans. Smart Grid 11 (2020) 1112–1123, https://doi.org/10.1109/TSG.2019.2932057.
[4] B.J. Kalkbrenner, Residential vs. community battery storage systems – consumer preferences in Germany, Energy Policy 129 (2019) 1355–1363, https://doi.org/10.1016/j.enpol.2019.03.041.
[5] D. Hettiarachchi, S. Shing Choi, S. Rajakaruna, A. Ghosh, Development of control strategy for community battery energy storage system in grid-connected microgrid of high photovoltaic penetration level, Int. J. Electr. Power Energy Syst. 155 (2024) 109527, https://doi.org/10.1016/j.ijepes.2023.109527.
[6] J. Jo, J. Park, Demand-side management with shared energy storage system in smart grid, IEEE Trans. Smart Grid 11 (2020) 4466–4476, https://doi.org/10.1109/TSG.2020.2980318.
[7] Y. Wang, H. Wang, M. Wagner, A. Liebman, Community Battery Energy Storage Systems for Enhancing Distribution System Operation: A Multi-objective Optimization Approach, 2023, https://doi.org/10.48550/arXiv.2311.16110.
[8] Y. Liu, Y. Wang, H. Xi, J. Lin, J. Ma, Community energy cooperation with shared energy storage for economic-environment benefits, in: 2022 IEEE PES Innovative Smart Grid Technologies - Asia (ISGT Asia), 2022, pp. 230–234, https://doi.org/10.1109/ISGTAsia54193.2022.10003636.
[9] F. Calero, C.A. Cañizares, K. Bhattacharya, C. Anierobi, I. Calero, M.F.Z. De Souza, M. Farrokhabadi, N.S. Guzman, W. Mendieta, D. Peralta, B.V. Solanki, N. Padmanabhan, W. Violante, A review of modeling and applications of energy storage systems in power grids, Proc. IEEE 111 (2023) 806–831, https://doi.org/10.1109/JPROC.2022.3158607.
[10] D.L. Rodrigues, X. Ye, X. Xia, B. Zhu, Battery energy storage sizing optimisation for different ownership structures in a peer-to-peer energy sharing community, Appl. Energy 262 (2020) 114498, https://doi.org/10.1016/j.apenergy.2020.114498.
[11] F. Hafiz, A. Rodrigo De Queiroz, P. Fajri, I. Husain, Energy management and optimal storage sizing for a shared community: a multi-stage stochastic programming approach, Appl. Energy 236 (2019) 42–54, https://doi.org/10.1016/j.apenergy.2018.11.080.
[12] H. Kang, S. Jung, H. Kim, J. Hong, J. Jeoung, T. Hong, Multi-objective sizing and real-time scheduling of battery energy storage in energy-sharing community based on reinforcement learning, Renew. Sust. Energ. Rev. 185 (2023) 113655, https://doi.org/10.1016/j.rser.2023.113655.
[13] N.T. Dinh, S. Karimi-Arpanahi, S.A. Pourmousavi, M. Guo, J.A.R. Liisberg, Cost-effective community battery sizing and operation within a local market framework, Policy and Regulation IEEE Transactions on Energy Markets 1 (2023) 536–548, https://doi.org/10.1109/TEMPR.2023.3324798.
[14] V.K. Saini, R. Kumar, A.S. Al-Sumaiti, B.K. Panigrahi, Uncertainty aware optimal battery sizing for cloud energy storage in community microgrid, Electr. Power Syst. Res. 222 (2023) 109482, https://doi.org/10.1016/j.epsr.2023.109482.
[15] R.V. Morcilla, N.H. Enano, Sizing of community centralized battery energy storage system and aggregated residential solar PV system as virtual power plant to support electrical distribution network reliability improvement, Renewable Energy Focus 46 (2023) 27–38, https://doi.org/10.1016/j.ref.2023.05.007.
[16] Y. Yang, G. Hu, C.J. Spanos, Optimal sharing and fair cost allocation of community energy storage, IEEE Trans. Smart Grid 12 (2021) 4185–4194, https://doi.org/10.1109/TSG.2021.3083882.
[17] T. Weckesser, D.F. Dominković, E.M.V. Blomgren, A. Schledorn, H. Madsen, Renewable energy communities: optimal sizing and distribution grid impact of photo-voltaics and battery storage, Appl. Energy 301 (2021) 117408, https://doi.org/10.1016/j.apenergy.2021.117408.
[18] N. Zhang, H. Jiang, E. Du, Z. Zhuo, P. Wang, Z. Wang, Y. Zhang, An efficient power system planning model considering year-round hourly operation simulation, IEEE Trans. Power Syst. 37 (2022) 4925–4935, https://doi.org/10.1109/TPWRS.2022.3146299.
[19] P. Gabrielli, M. Gazzani, E. Martelli, M. Mazzotti, Optimal design of multi-energy systems with seasonal storage, Appl. Energy 219 (2018) 408–424, https://doi.org/10.1016/j.apenergy.2017.07.142.
[20] L. Kotzur, P. Markewitz, M. Robinius, D. Stolten, Time series aggregation for energy system design: modeling seasonal storage, Appl. Energy 213 (2018) 123–135, https://doi.org/10.1016/j.apenergy.2018.01.023.
[21] M. Elkazaz, M. Sumner, E. Naghiyev, Z. Hua, D.W.P. Thomas, Techno-economic sizing of a community battery to provide community energy billing and additional ancillary services, Sustainable Energy, Grids and Networks 26 (2021) 100439, https://doi.org/10.1016/j.segan.2021.100439.
[22] J. Yang, T.K. Saha, M.R. Alam, W. Tushar, Transactive control of community batteries for voltage regulation in distribution systems, J. Energy Storage 90 (2024) 111798, https://doi.org/10.1016/j.est.2024.111798.
[23] M. Kazemi, H. Zareipour, N. Amjady, W.D. Rosehart, M. Ehsan, Operation scheduling of battery storage systems in joint energy and ancillary services markets, IEEE Trans. Sustain. Energy 8 (2017) 1726–1735, https://doi.org/10.1109/TSTE.2017.2706563.

[24] J. Lin, J. Sun, Y. Feng, M. Zheng, Z. Yu, Aggregate demand response strategies for smart communities with battery-charging/switching electric vehicles, J. Energy Storage 58 (2023) 106413, https://doi.org/10.1016/j.est.2022.106413.
[25] A. Biancardi, C. Mendes, I. Staffell, Battery electricity storage as both a complement and substitute for cross-border interconnection, Energy Policy 189 (2024) 114134, https://doi.org/10.1016/j.enpol.2024.114134.
[26] Z. Csereklyei, S. Dwyer, A. Kallies, D. Economou, The role of community-scale batteries in the energy transition: case studies from Australia's National Electricity Market, J. Energy Storage 93 (2024) 112277, https://doi.org/10.1016/j.est.2024.112277.
[27] S. Ye, J. Wang, Z. Yin, J. Kang, Z. Ma, Optimization of a solar-driven community integrated energy system based on dynamic hybrid hydrogen-electric energy storage strategy, Journal of Energy Storage 101 (2024) 113917, https://doi.org/10.1016/j.est.2024.113917.
[28] M.A. Khan, T. Rehman, A. Hussain, H.-M. Kim, Day-ahead operation of a multi-energy microgrid community with shared hybrid energy storage and EV integration, Journal of Energy Storage 97 (2024) 112855, https://doi.org/10.1016/j.est.2024.112855.
[29] Z. Liu, Y. Li, G. Fan, D. Wu, J. Guo, G. Jin, S. Zhang, X. Yang, Co-optimization of a novel distributed energy system integrated with hybrid energy storage in different nearly zero energy community scenarios, Energy 247 (2022) 123553, https://doi.org/10.1016/j.energy.2022.123553.
[30] S. Sahoo, P. Timmann, Energy storage technologies for modern power systems: a detailed analysis of functionalities, potentials, and impacts, IEEE, Access 11 (2023) 49689–49729, https://doi.org/10.1109/ACCESS.2023.3274504.
[31] O. Dumont, V. Lemort, Mapping of performance of pumped thermal energy storage (Carnot battery) using waste heat recovery, Energy 211 (2020) 118963, https://doi.org/10.1016/j.energy.2020.118963.
[32] M.T. Ameen, Z. Ma, A. Smallbone, R. Norman, A.P. Roskilly, Demonstration system of pumped heat energy storage (PHES) and its round-trip efficiency, Appl. Energy 333 (2023) 120580, https://doi.org/10.1016/j.apenergy.2022.120580.
[33] Australian Renewable Energy Agency, Community batteries: a cost/benefit analysis. https://arena.gov.au/knowledge-bank/community-batteries-a-cost-benefit-analysis/, 2021. (Accessed 30 July 2024).
[34] B.P. Koirala, E. van Oost, H. van der Windt, Community energy storage: a responsible innovation towards a sustainable energy system? Appl. Energy 231 (2018) 570–585, https://doi.org/10.1016/j.apenergy.2018.09.163.
[35] R. Kapoor, R. Gupta, L.H. Son, S. Jha, R. Kumar, Boosting performance of power quality event identification with KL Divergence measure and standard deviation, Measurement 126 (2018) 134–142, https://doi.org/10.1016/j.measurement.2018.05.053.
[36] S. Sharma, M. Mortazavi, Pumped thermal energy storage: a review, Int. J. Heat Mass Transf. 213 (2023) 124286, https://doi.org/10.1016/j.ijheatmasstransfer.2023.124286.
[37] Y. Wu, Z. Liu, J. Liu, H. Xiao, R. Liu, L. Zhang, Optimal battery capacity of grid-connected PV-battery systems considering battery degradation, Renew. Energy 181 (2022) 10–23, https://doi.org/10.1016/j.renene.2021.09.036.
[38] S. Touzani, A.K. Prakash, Z. Wang, S. Agarwal, M. Pritoni, M. Kiran, R. Brown, J. Granderson, Controlling distributed energy resources via deep reinforcement learning for load flexibility and energy efficiency, Appl. Energy 304 (2021) 117733, https://doi.org/10.1016/j.apenergy.2021.117733.
[39] X. Ma, F. Liu, Y. Qi, X. Wang, L. Li, L. Jiao, M. Yin, M. Gong, A multiobjective evolutionary algorithm based on decision variable analyses for multiobjective optimization problems with large-scale variables, IEEE Trans. Evol. Comput. 20 (2016) 275–298, https://doi.org/10.1109/TEVC.2015.2455812.
[40] B. Cortés-Caicedo, J. Ocampo-Toro, R.I. Bolaños, O.D. Montoya, L.F. Grisales-Noreña, A multi-objective PSO for DC microgrids: efficient battery management to minimize energy losses and operating costs, J. Energy Storage 96 (2024) 112550, https://doi.org/10.1016/j.est.2024.112550.
[41] E.L. Ratnam, S.R. Weller, C.M. Kellett, A.T. Murray, Residential load and rooftop PV generation: an Australian distribution network dataset, Int. J. Sustainable Energy 36 (2017) 787–806, https://doi.org/10.1080/14786451.2015.1100196.
[42] Australian Energy Market Operator, Wholesale electricity market data. https://aemo.com.au/energy-systems/electricity/wholesale-electricity-market-wem/data-wem/market-data-wa, 2023. (Accessed 30 July 2024).
[43] F. Bilendo, H. Badihi, N. Lu, P. Cambron, B. Jiang, A normal behavior model based on power curve and stacked regressions for condition monitoring of wind turbines, IEEE Trans. Instrum. Meas. 71 (2022) 1–13, https://doi.org/10.1109/TIM.2022.3196116.
[44] C. Zhang, W. Yin, T. Wen, An advanced multi-objective collaborative scheduling strategy for large scale EV charging and discharging connected to the predictable wind power grid, Energy 287 (2024) 129495, https://doi.org/10.1016/j.energy.2023.129495.
[45] Y.Q. Ge, Y. Zhao, C.Y. Zhao, Transient simulation and thermodynamic analysis of pumped thermal electricity storage based on packed-bed latent heat/cold stores, Renew. Energy 174 (2021) 939–951, https://doi.org/10.1016/j.renene.2021.04.094.
[46] A. Benato, Performance and cost evaluation of an innovative Pumped Thermal Electricity Storage power system, Energy 138 (2017) 419–436, https://doi.org/10.1016/j.energy.2017.07.066.
[47] S. Hu, Z. Yang, J. Li, Y. Duan, Thermo-economic analysis of the pumped thermal energy storage with thermal integration in different application scenarios, Energy Convers. Manag. 236 (2021) 114072, https://doi.org/10.1016/j.enconman.2021.114072.
[48] Z. Zheng, X. Li, J. Pan, X. Luo, A multi-year two-stage stochastic programming model for optimal design and operation of residential photovoltaic-battery systems, Energ. Buildings 239 (2021) 110835, https://doi.org/10.1016/j.enbuild.2021.110835.
[49] S. Orangi, N. Manjong, D.P. Clos, L. Usai, O.S. Burheim, A.H. Strømman, Historical and prospective lithium-ion battery cost trajectories from a bottom-up production modeling perspective, J. Energy Storage 76 (2024) 109800, https://doi.org/10.1016/j.est.2023.109800.